

1 Towards a Pixel TPC part I: construction and test of a  
2 32-chip GridPix detector

3 M. van Beuzekom<sup>a</sup>, Y. Bilevych<sup>b</sup>, K. Desch<sup>b</sup>, S. van Doesburg<sup>a</sup>,  
4 H. van der Graaf<sup>a</sup>, F. Hartjes<sup>a</sup>, J. Kaminski<sup>b</sup>, P.M. Kluit<sup>a</sup>,  
5 N. van der Kolk<sup>a</sup>, C. Ligtenberg<sup>a</sup>, G. Raven<sup>a</sup>, J. Timmermans<sup>a</sup>

6 <sup>a</sup>*Nikhef, Science Park 105, 1098 XG Amsterdam, The Netherlands*

7 <sup>b</sup>*Physikalisches Institut, University of Bonn, Nussallee 12, 53115 Bonn,*  
8 *Germany*

---

9 **Abstract**

10 A Time Projection Chamber (TPC) module with 32 GridPix chips was con-  
11 structed and the performance was measured using data taken in a testbeam  
12 at DESY in 2021. The GridPix chips each consist of a Timepix3 ASIC  
13 (TPX3) with an integrated amplification grid and have a high efficiency of  
14 about 85% to detect single ionisation electrons. In the testbeam setup, the  
15 module was placed in between two sets of Mimosas26 silicon detector planes  
16 that provided external high-precision tracking and the whole detector setup  
17 was slid into the PCMAG magnet at DESY. The TPC could be operated  
18 reliably and used a 93.6/5.0/1.4 gas mixture (by volume) of Ar/iC<sub>4</sub>H<sub>10</sub>/CO<sub>2</sub>  
19 with a small amount of oxygen and water vapour. The analysed data were  
20 taken at electron beam momenta of 5 and 6 GeV/c and at magnetic fields of  
21 0 and 1 T.

22 The result for the transverse diffusion coefficient  $D_T$  is  $(287.2 \pm 0.5)$   
23  $\mu\text{m}/\sqrt{\text{cm}}$  at  $B = 0$  T and  $D_T$   $(120.3 \pm 0.5) \mu\text{m}/\sqrt{\text{cm}}$  at  $B = 1$  T. The  
24 longitudinal diffusion coefficient  $D_L$  is measured to be  $(251 \pm 14) \mu\text{m}/\sqrt{\text{cm}}$

---

\*Corresponding author, Telephone: +31 20 592 2000  
*Preprint submitted to Nuclear Instruments and Methods A*  
Email address: s01@nikhef.nl (P.M. Kluit)

25 at  $B = 0$  T and  $(224 \pm 14) \mu\text{m}/\sqrt{\text{cm}}$  at  $B = 1$  T. Results for the tracking  
26 systematical uncertainties in  $xy$  (pixel plane) were measured to be smaller  
27 than  $13 \mu\text{m}$  with and without magnetic field. The tracking systematical  
28 uncertainties in  $z$  (drift direction) were smaller than  $15 \mu\text{m}$  ( $B = 0$  T) and  
29  $20 \mu\text{m}$  ( $B = 1$  T).

30 *Keywords:*

31 Micromegas, gaseous pixel detector, micro-pattern gaseous detector,  
32 Timepix, GridPix, pixel time projection chamber

---

## 33 1. Introduction

34 Earlier publications on a single chip [1] and four chip (quad) GridPix de-  
35 tectors [2] showed the potential of the GridPix technology and the large range  
36 of applications for these devices [3]. In particular, it was demonstrated that  
37 single ionisation electrons can be detected with high efficiency and accuracy,  
38 allowing excellent 3D track position measurements and particle identification  
39 based on the number of electrons and clusters.

40 As a next step towards a Pixel Time Projection Chamber for a future  
41 collider experiment [4, 5], a module consisting of 32 GridPix chips based on  
42 the TPX3 chip was constructed.

43 A GridPix detector consists of a CMOS pixel TPX3 chip [6] with inte-  
44 grated amplification grid added by photo-lithographic - Micro-electromechanical  
45 Systems (MEMS) - post-processing techniques. The TPX3 chip can be op-  
46 erated with a low threshold of  $515 e^-$ , and has a low equivalent noise charge  
47 of about  $70 e^-$ . The GridPix single chip and quad detectors have a very  
48 fine granularity of  $55 \times 55 \mu\text{m}^2$  with  $256 \times 256$  pixels per chip. The device has

49 a high efficiency of about 85% - discussed in this paper - to detect single  
50 ionisation electrons.

51 Based on the experience gained with these detectors a 32-GridPix detector  
52 module - consisting of 8 quad detectors - was built. A drift box defining the  
53 electric field and gas envelope was constructed. A read out system for up  
54 to 128 chips with 4 multiplexers read out by one Speedy Pixel Detector  
55 Readout (SPIDR) board [7, 8] was designed. After a series of tests using  
56 the laser setup [9] and cosmics in the laboratory at Nikhef, the detector was  
57 taken to DESY for a two week testbeam campaign.

58 At DESY, the 32-chip detector was placed in between two sets of Mi-  
59 mosa26 silicon detector planes and mounted on a movable stage. The whole  
60 detector setup was slid into the centre of the PCMAG magnet at DESY.  
61 A beam trigger was provided by scintillator counters. The data reported  
62 here were taken at different stage positions and electron beam momenta of  
63 5 and 6 GeV/c and at magnetic fields of 0 and 1 T. The performance of the  
64 32-GridPix detector module was measured using these data sets.

65 In this paper, part I of the results will be presented with the main focus on  
66 the detector spatial resolution and tracking performance. A second follow-up  
67 paper will discuss the  $dE/dx$  (or  $dN/dx$ ) and other results.

## 68 **2. The 32-GridPix detector module**

69 A 32-GridPix detector module was built using the quad detector module  
70 [2] as a basic building block. The quad module consists of four GridPix chips  
71 and is optimised for a high fraction of sensitive area of 68.9%. The external  
72 dimensions are 39.60 mm  $\times$  28.38 mm. The four chips which are mounted

73 on a cooled base plate (COCA), are connected with wire bonds to a common  
74 central 6 mm wide PCB. A 10 mm wide guard electrode is placed over the  
75 wire bonds 1.1 mm above the aluminium grids, in order to prevent field  
76 distortions of the electric drift field. The guard electrode is the main inactive  
77 area, and its dimensions are set by the space required for the wire bonds.  
78 On the back side of the quad module, the PCB is connected to a low voltage  
79 regulator. The aluminium grids of the GridPix detectors are connected by  
80 80  $\mu\text{m}$  insulated copper wires to a high voltage (HV) filtering board. The  
81 quad module consumes about 8 W of power of which 2 W is used in the LV  
82 regulator.

83 Eight quad modules were embedded in a box, resulting in a GridPix  
84 detector module with a total of 32 chips. A schematic 3-dimensional drawing  
85 of the detector is shown in Figure 1. A schematic drawing of the quad  
86 detectors in the module is shown in Figure 2, where also the beam direction  
87 is indicated.

88 The internal dimensions of the box are 79 mm along the  $x$ -axis, 192 mm  
89 along the  $y$ -axis, and 53 mm along the  $z$ -axis (drift direction), and it has a  
90 maximum drift length (distance between cathode and read out anode) of 40  
91 mm. The drift field is shaped by a series of parallel CuBe field wires of 75  
92  $\mu\text{m}$  diameter with a wire pitch of 2 mm. Guard strips are located on all of  
93 the four sides of the active area. In addition, six guard wires - shown with  
94 dashed lines (one colored red) in Figure 2 - are suspended over the boundaries  
95 of the chips, to minimise distortions of the electric drift field. The wires are  
96 located at a distance of 1.15 mm from the grid planes, and their potential is  
97 set to the drift potential at this drift distance. The box has two 50  $\mu\text{m}$  thick

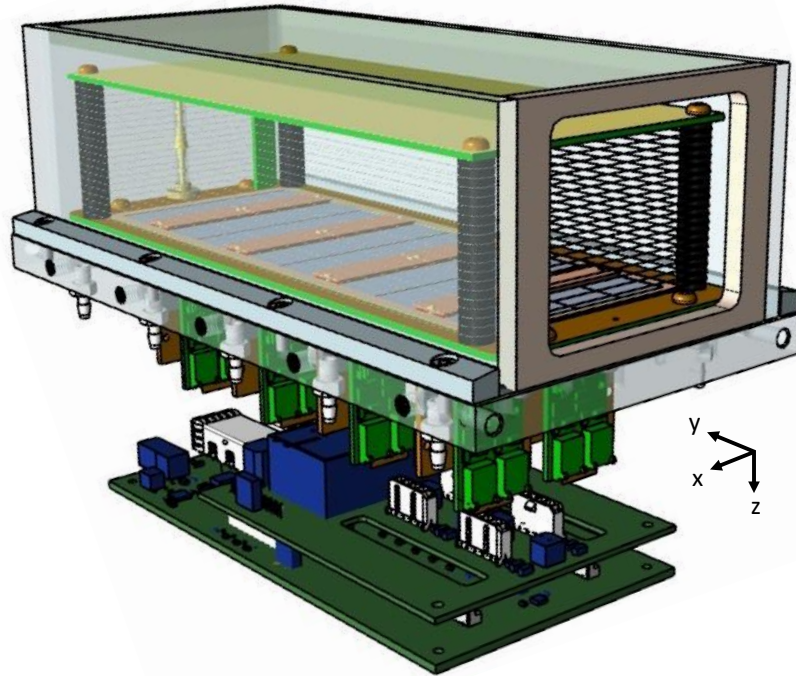


Figure 1: Schematic 3-dimensional rendering of the 32-GridPix module detector for illustration purposes.

98 Kapton windows to allow the beam to pass with minimal multiple scattering.  
 99 The gas volume of 780 ml is continuously flushed at a rate of  $\sim 50$  ml/min  
 100 (about 4 volumes/hour) with premixed T2K TPC gas. This gas is a mixture  
 101 consisting of 95% Ar, 3%  $\text{CF}_4$ , and 2%  $\text{iC}_4\text{H}_{10}$  suitable for large TPCs because  
 102 of the low transverse diffusion in a magnetic field and the high drift velocity.  
 103 The data acquisition system of the quad module was adopted to allow for  
 104 reading out multiple quad detectors. A multiplexer card was developed that  
 105 handles four quad detectors or 16 chips and combines the TPX3 data into  
 106 one data stream. For the 32-GridPix module two multiplexers are connected  
 107 to a SPIDR board that controls the chips and read out process. The read

108 out speed per chip is 160 Mbps and for the multiplexer 2.56 Gbps: this  
 109 corresponds to a maximum rate of 21 MHits/s. For each pixel the precise  
 110 Time of Arrival (ToA) using a 640 MHz TDC and the time over threshold  
 111 (ToT) are measured.

### 112 3. Experimental setup

113 In preparation of the two weeks DESY testbeam campaign, a support  
 114 frame was designed to move the 32-chip GridPix detector module in the  
 115 plane perpendicular to the beam by a remotely controlled stage such that  
 116 the whole detector volume could be probed. The module was mounted upside  
 117 down with respect to Figure 1 to allow access to the electronics from above.

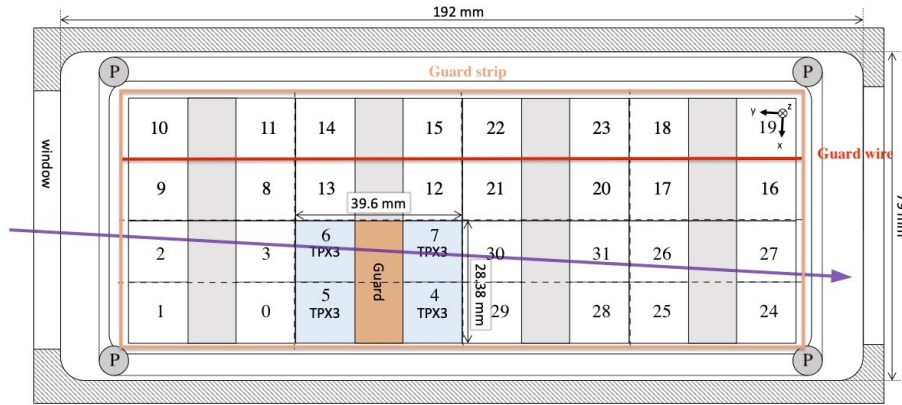


Figure 2: Schematic drawing of the 32-GridPix module detector with one example quad as viewed from the top of the quad detectors. The chips are numbered and the beam direction is shown in purple. A guard electrode of a quad detector is shown in orange. The four surrounding guard strips are shown -not to scale- in orange. Six guard wires - are shown with dashed lines (one colored red) and the pillars of the drift box are shown as circles with a P in the centre.

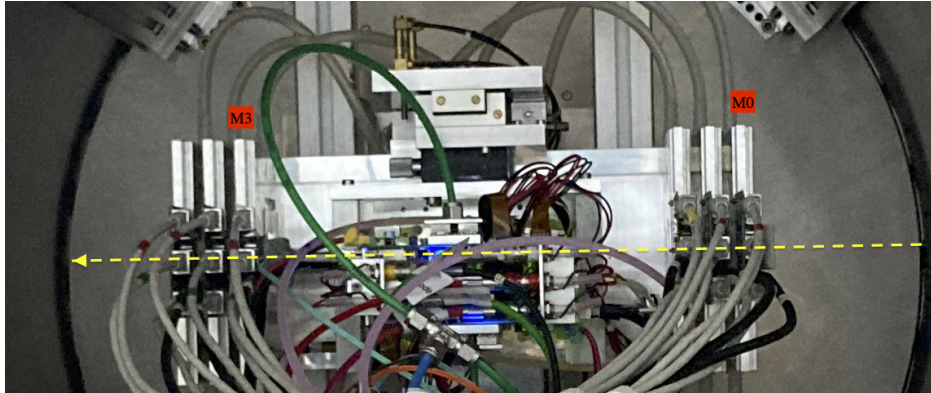


Figure 3: Photo of the detector setup - side view - at the centre of the PCMAG magnet (the circular contour). The Mimosa26 planes M0 and M3 are indicated in red as well as the beam direction (yellow).

118 The support frame also held three Mimosa26 silicon detector planes [10] -  
119 with an active area of  $(21.2 \text{ mm} \times 10.6 \text{ mm})$  - placed in front of the detector  
120 and three Mimosa26 planes behind the detector. At DESY, the Mimosa26  
121 silicon detector planes were provided by the testbeam coordinators. The  
122 whole detector setup was slid towards the centre of the PCMAG magnet  
123 at the DESY II testbeam facility [10]. A beam trigger was provided by a  
124 double scintillator counter coincidence. The data were taken at different  
125 stage positions to cover the whole sensitive TPC volume. Runs with electron  
126 beam momenta of 5 and 6 GeV/c and at magnetic fields of 0 and 1 T were  
127 analysed.

128 A photograph of the detector setup in the PCMAG magnet is shown in  
129 Figure 3. The stage positions of the TPC module with respect to the beam  
130 and the Mimosa26 planes can be adjusted.

131 The experimental and environmental parameters such as temperature,

132 pressure, gas flow and oxygen content were measured and logged by a Win-  
 133 dows operated slow control system. The experimental parameters are sum-  
 134 marised in Table 1. The chips were cooled by circulating Glycol through  
 135 the cooling channels in the module carrier plate. The cooling blocks of the  
 136 multiplexers were further cooled by blowing pressurised air on them.

Table 1: Overview of the experimental parameters. The ranges indicate the variation over the data taking period

|  |                    |
|--|--------------------|
| Number of analysed runs at $B=0$ (1) T | 6 (8)              |
| Run duration                           | 10-90 minutes      |
| Number of triggers per run             | 3-100 k            |
| $E_{\text{drift}}$                     | 280 V/cm           |
| $V_{\text{grid}}$                      | 340 V              |
| Threshold                              | 550 e <sup>-</sup> |
| Gas temperature                        | 303.3-306.6 K      |
| Pressure                               | 1011 – 1023 mbar   |
| Oxygen concentration                   | 240 - 620 ppm      |
| Water vapour concentration             | 2000 - 7000 ppm    |

137 The data was produced in four main data streams: one stream produced  
 138 by the Mimosa26 telescope, two data streams by the two Timepix multiplex-  
 139 ers and one trigger stream. The double scintillator coincidence provided a  
 140 trigger signal to the Trigger Logic Unit (TLU) [11] that sends a signal to the  
 141 telescope read out and the trigger SPIDR. The data acquisition systems of  
 142 the telescope and trigger SPIDR injected a time stamp into their respective  
 143 data streams. Hits from the Mimosa26 planes were collected with a sliding



144 window of  $-115 \mu\text{s}$  to  $230 \mu\text{s}$  around the trigger time. The data acquisition  
145 of the multiplexer and the trigger SPIDR were synchronised at the start of  
146 the run. By comparing the time stamps in these streams, telescope tracks  
147 and TPC tracks could be matched. Unfortunately, the SPIDR trigger had  
148 - due to a cabling mistake at the output of the TLU - a common 25 ns flat  
149 time jitter.

150 After a short data taking period one of the chips (nr 11) developed a  
151 short circuit and the HV on the grid of the chip was disconnected. After the  
152 testbeam data taking period the module was repaired in the clean room in  
153 Bonn.

## 154 4. Analysis

### 155 4.1. Telescope track reconstruction procedure

156 The data of the telescope is decoded and analysed using the Corryvreckan  
157 software package [12]. The track model used for fitting was the General  
158 Broken Lines (GBL) software [14]. The code was extended and optimised to  
159 fit curved broken lines for the data with magnetic field. The telescope planes  
160 were iteratively aligned using the standard alignment software provided by  
161 the package. The single point Mimosas26 resolution is  $4 \mu\text{m}$  in  $x$  and  $6 \mu\text{m}$   
162 in  $z$  (drift direction) [10].

163 Telescope tracks were required to have hits in at least 5 out of the 6 planes  
164 and a total  $\chi^2$  of better than 25 per degree of freedom. The uncertainties on  
165 the telescope track prediction in the middle of the GridPix detector module  
166 are dominated by multiple scattering. The amount of multiple scattering  
167 was estimated by comparing the predictions from the two telescope arms for

168 6 GeV/c tracks at  $B = 0$  T. The expected uncertainty in  $x$  and  $z$  is  $26 \mu\text{m}$   
169 on average.

#### 170 4.2. TPC Track reconstruction procedure

171 GridPx hits are selected requiring a minimum time over threshold ToT  
172 of  $0.15 \mu\text{s}$ . The drift time is defined as the measured time of arrival minus  
173 the trigger time recorded in the trigger SPIDR data stream minus a fixed  $t_0$   
174 (the drift time at zero drift). The drift time was corrected for time walk [2]  
175 using the measured time over threshold (ToT in units of  $\mu\text{s}$ ) and the formula  
176 (1):

$$\delta t = \frac{18.6(ns \mu s)}{\text{ToT} + 0.1577(\mu s)}. \quad (1)$$

177 Furthermore, small time shift corrections - with an odd-even and a  $16 \times$  pixels  
178 structure - coming from the TPX3 clock distribution were extracted from the  
179 data and applied.

180 The  $z$  drift coordinate was calculated as the product of the drift time  
181 and the drift velocity. This implies that  $z_{\text{drift}} = -z$  as defined in Figure 1.  
182 GridPix hits outside an acceptance window of 30 mm wide in  $x$  and 15 mm  
183 wide in  $z$ , corresponding to the size of the entrance window, were not used  
184 in the track finding and reconstruction. Based on a Hough transform an  
185 estimate of the TPC track position and angles in the middle of the module  
186 (at  $y = 1436$  pixels) were obtained. This estimate was used to collect the hits  
187 around the TPC track and fit the track parameters. For this fit a linear (for  
188  $B = 0$  T data) or a quadratic track (for  $B = 1$  T data) model was used. In  
189 the fit, the expected uncertainties per hit  $\sigma_{xy}$  and  $\sigma_z$  were used. The expected

Table 2: Table with track/event selection cuts

| Track/Event Selection  |
|--|
| $ x_{\text{TPC}} - x_{\text{telescope}}  < 0.3 \text{ mm}$         |
| $ z_{\text{TPC}} - z_{\text{telescope}}  < 2 \text{ mm}$           |
| $ dx/dy_{\text{TPC}} - dx/dy_{\text{telescope}}  < 4 \text{ mrad}$ |
| $ dz/dy_{\text{TPC}} - dz/dy_{\text{telescope}}  < 2 \text{ mrad}$ |

190 uncertainties were derived using the parametrisations discussed in section 5.  
 191 The fit was iterated three times to reject outlier hits at respectively 10, 5  
 192 and 2.5 sigma. A TPC track was required to have at least 100 hits in each  
 193 multiplexer. At least 25% of the total number of hits should be on track and  
 194 the  $\chi^2$  per degree of freedom had to be less than 3 in  $xy$  and  $zy$ . All track  
 195 parameters were expressed at a plane in the middle of the TPC module.

196 The calibration and alignment of the detector was done using high quality  
 197 tracks for which the track selections are summarised in Table 2.

198 The drift velocity was calibrated per run by fitting a linear function to  
 199 the  $z$  (predicted from the telescope track at the measured TPC hit position)  
 200 versus the measured drift time in the TPC. For the  $B = 0$  T runs it varies  
 201 between 61.6 and 63.0  $\mu\text{m}/\text{ns}$ . For the  $B = 1$  T runs it is between 57.2 and  
 202 59.1  $\mu\text{m}/\text{ns}$ . The variation comes mainly from the changes in the relative  
 203 humidity of the gas volume due to small leaks.

204 The individual TPX3 chips were iteratively aligned fitting a shift in  $x$  ( $z$ )  
 205 and two slopes  $dx(z)/dx(y)$ . The alignment was done per run, because the  
 206 detector was moved in  $x$  and/or  $z$  for each run. The fitted slopes were also  
 207 corrected for small shifts and rotations (3D) in the nominal chip position.

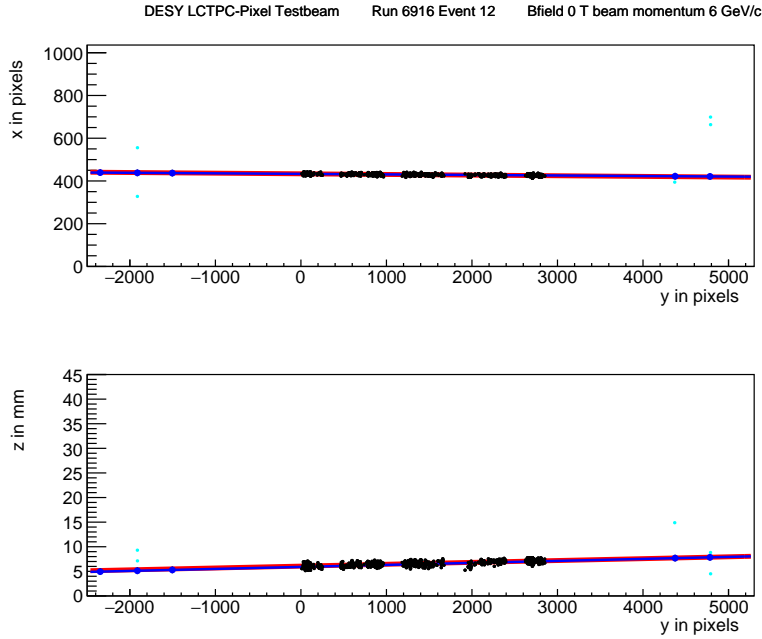


Figure 4: An event display for run 6916 without  $B$  field, with in total 1293 TPC hits (black dots) in the (top) precision plane  $(x, y)$  and (bottom) drift plane  $(z \text{ drift}, y)$ . The fitted TPC track (red line) with 1130 hits on track and the telescope track (blue line) with 5 Mimosas26 planes (blue hits) on track are shown. In green the off track Mimosas26 hits are shown.

208     An example event from run 6916 without  $B$  field with a TPC and a  
 209     telescope track is shown in Figure 4. The TPC is located between  $y = 0$  and  
 210     2872 pixels. Three Mimosas26 planes are located at  $y < -1000$  and three at  
 211      $y > 4000$  pixels.

## 212    5. Hit resolutions

213     The track residual in  $xy$  is defined as the closest distance - defined as the  
 214     2D  $xy$  projection of the 3D distance - between the hit at the center of the

215 pixel and the track. The residual in  $z$  is calculated at this point of closest  
 216 approach. The single-electron hit resolutions in  $xy$  and  $z$  will be extracted  
 217 from the track residuals. In order to study the single-electron resolution  
 218 for the data with and without magnetic field, additional selections on the  
 219 telescope and TPC tracks were applied. Due to the trigger time jitter of 25  
 220 ns (corresponding to 1.5 mm drift), the prediction of the telescope track in  
 221  $z$  must be used as the reference for  $z$ . Therefore the  $z$  hits of the TPC track  
 222 were fitted to correct for the common time shift and the - biased -  $z$  residuals  
 223 were calculated with respect to the fitted TPC track. In the  $xy$  plane the  
 224 residuals of TPC hits with respect to the telescope track were used to extract  
 225 the single-electron resolution in  $xy$ . For the resolution studies, runs at three  
 226 different  $z$  stage positions of the TPC were selected where the beam gave  
 227 hits in the central chips. The data of 14 central chips (9, 12, 21, 20, 17, 16,  
 228 2, 3, 6, 7, 30, 31, 26 and 27) were used. Two chips (8 and 13) were left out  
 229 because of the E field deformations caused by the short circuit in chip 11.

### 230 5.1. Hit resolutions in the pixel plane

231 The residual of the hits in the pixel plane ( $xy$ ) was measured as a function  
 232 of the predicted drift position ( $z_{\text{drift}}$ ). Tracks were selected that crossed the  
 233 fiducial region defined by the central core of the beam. Hits were removed  
 234 in a region of 20 pixels near the chip edges in  $x$ . The spread on the residual  
 235 in  $xy$  for an ionisation electron is given by:

$$\sigma_{xy}^2 = \sigma_{\text{track}}^2 + \frac{d_{\text{pixel}}^2}{12} + D_T^2(z_{\text{drift}} - z_0), \quad (2)$$

236 where  $\sigma_{\text{track}}$  is the uncertainty from the track prediction,  $d_{\text{pixel}}$  is the pixel  
 237 pitch size,  $z_0$  is the position of the grid, and  $D_T$  is the transverse diffusion

238 coefficient. The last two terms correspond to the single-electron detector  
 239 resolution (squared). The resolution at zero drift distance  $d_{\text{pixel}}/\sqrt{12}$  was  
 240 fixed to  $15.9 \mu\text{m}$  and  $\sigma_{\text{track}}$  to  $30 \mu\text{m}$  for  $B = 0 \text{ T}$  and  $42 \mu\text{m}$  for  $B =$   
 241  $1 \text{ T}$  data. The uncertainty on the track prediction was measured and is  
 242 larger than the Mimosa plane resolution because of multiple scattering in  
 243 the sensors and in the entrance and exit windows.

244 The expression (2) - leaving  $z_0$  and  $D_T$  as free parameters - is fitted  
 245 to the  $B = 0 \text{ T}$  data shown in Figure 5. The fit gives a transverse diffusion  
 246 coefficient  $D_T$  of  $(287.2 \pm 0.5) \mu\text{m}/\sqrt{\text{cm}}$ . The measured value is in agreement  
 247 with the value of  $287 \mu\text{m}/\sqrt{\text{cm}} \pm 4\%$  predicted by the gas simulation software  
 248 Magboltz 11.9 [15]. The values of the diffusion coefficients depend on the  
 249 humidity that was not precisely measured during the testbeam. The humidity  
 250 strongly affects the drift velocity. Therefore the drift velocity prediction from  
 251 Magboltz was used to determine the water content per run and predictions  
 252 for the diffusion coefficients could be obtained.

253 A fit to the  $B = 1 \text{ T}$  data, also shown in Figure 5, gives a transverse  
 254 diffusion coefficient  $D_T$  of  $(120.3 \pm 0.5) \mu\text{m}/\sqrt{\text{cm}}$ . The measured value is in  
 255 agreement with the value of  $119 \mu\text{m}/\sqrt{\text{cm}} \pm 2\%$  predicted by Magboltz.

## 256 5.2. Hit resolution in the drift plane

257 The spread on the residual in  $z$  of the ionisation electrons  $\sigma_z$  is given by:

$$\sigma_z^2 = \sigma_{\text{track}}^2 + \sigma_{z_0}^2 + D_L^2(z_{\text{drift}} - z_0), \quad (3)$$

258 where  $\sigma_{\text{track}}$  is the expected track uncertainty,  $\sigma_{z_0}$  the detector resolution at  
 259 zero drift distance and  $D_L$  the longitudinal diffusion constant. The last two  
 260 terms in the equation correspond to the single-electron detector resolution

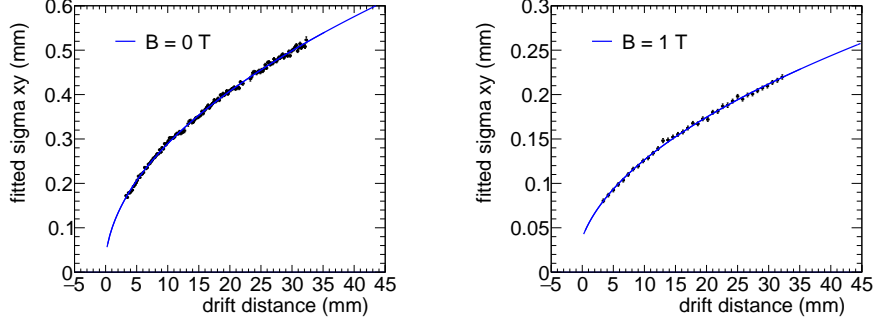


Figure 5: Measured spread on the residuals in the pixel plane (black points) for (left)  $B = 0$  T and (right)  $B = 1$  T, fitted with equation (2) (blue line).

261 (squared). Only tracks crossing the fiducial region - defined by the central  
 262 core of the beam - were accepted and hits with a ToT value above  $0.6 \mu\text{s}$   
 263 were selected. Because of the time jitter, the fitted TPC track is used for the  
 264 drift residuals. For  $z_{\text{drift}}$  the telescope prediction at the hit was used. The  
 265 expected uncertainty on TPC track prediction is propagated and amounts to  
 266  $50 \mu\text{m}$  at  $z = z_0$ . The systematic uncertainty on  $\sigma_{\text{track}}$  is estimated to be 25  
 267  $\mu\text{m}$ .

268 The expression (3) - leaving  $\sigma_{z_0}$  and  $D_L$  as free parameters - is fitted  
 269 to the  $B = 0$  T data shown in Figure 6. The value of  $z_0$  was fixed to the  
 270 result of the fit in the  $xy$  plane. The value of  $\sigma_{z_0}$  was measured to be 129  
 271  $\mu\text{m}$ . The longitudinal diffusion coefficient  $D_L$  was determined to be  $(251$   
 272  $\pm 1$  (stat)  $\pm 14$  (sys))  $\mu\text{m}/\sqrt{\text{cm}}$ , which is higher than the expected value  
 273  $236 \pm 3 \mu\text{m}/\sqrt{\text{cm}}$  from a Magboltz calculation [15]. The quoted systematic  
 274 uncertainty on  $D_L$  is rather large and obtained from a fit using  $\sigma_{\text{track}} = 25$   
 275  $\mu\text{m}$ .

276 A fit to the  $B = 1$  T data shown in Figure 6 gives a longitudinal diffusion

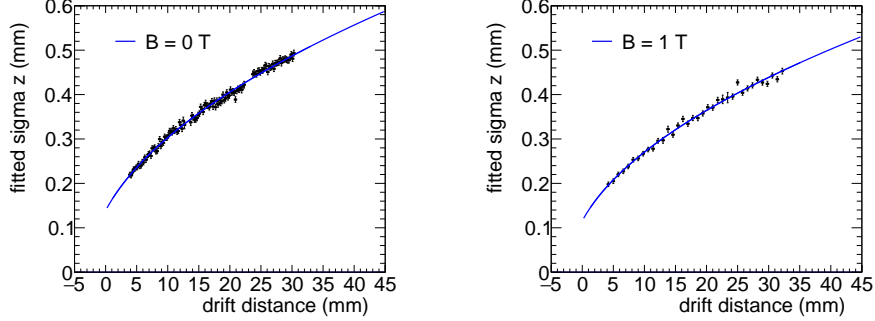


Figure 6: Measured spread on the residuals in the drift plane for hits with a ToT above  $0.60 \mu\text{s}$  for (left)  $B = 0 \text{ T}$  and (right)  $B = 1 \text{ T}$ . The data are fitted with the expression of equation (3).

277 coefficient  $D_L$  of  $(224 \pm 2 \text{ (stat)} \pm 14 \text{ (sys)}) \mu\text{m}/\sqrt{\text{cm}}$ . The measured value  
 278 is lower than the value of  $(245 \pm 4) \mu\text{m}/\sqrt{\text{cm}}$  predicted by Magboltz. The  
 279 fitted value of  $\sigma_{z0}$  was  $114 \mu\text{m}$ .

### 280 5.3. Deformations in the pixel and drift plane

281 It is important to measure possible deformations in the pixel ( $xy$ ) and  
 282 drift ( $z$ ) plane to quantify the tracking precision. For the construction of  
 283 a large Pixel TPC, deformations in the pixel plane should be controlled to  
 284 better than typically  $20 \mu\text{m}$  because these affect the momentum resolution.  
 285 The mean residuals in the pixel and drift planes are shown in Figure 7 for  
 286 the  $B = 0 \text{ T}$  data set using a large set of runs to cover the whole module.  
 287 The residuals were calculated with respect to the telescope track prediction.  
 288 Because of limited statistics, groups of  $16 \times 16$  pixels were combined into one  
 289 bin. Bins with less than 100 hits are left out and residuals larger (smaller)  
 290 than  $+(-)100 \mu\text{m}$  are shown in red (blue).



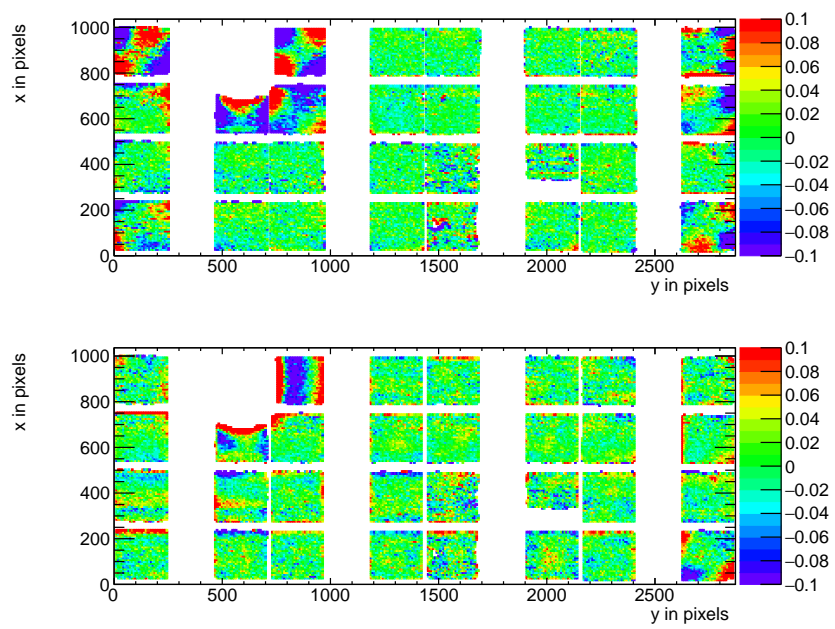


Figure 7: Mean residuals (color coded in mm) in the pixel (top) and drift (bottom) plane for  $B = 0$  T data at the expected hit position.

291 A few critical areas can be observed in Figure 7: the region around chip 11  
 292 is affected (chips 14, 8 and 13), because the grid of chip 11 was disconnected.  
 293 Deformations are present at the four corners of the drift box (chips 1, 10,  
 294 19 and 24) and close to the right upper corner edge (chip 16) of the drift  
 295 box. These come from inhomogeneities in the drift field near the supporting  
 296 pillars, where the field wires are too close to the chip to provide a constant  
 297 electric field. It was concluded that for the deformation studies the hits of  
 298 these nine chips have to be removed. The track fit was redone leaving these  
 299 hits out of the fit, such that they could not bias and affect the results. Note  
 300 that a bias in the mean residual at the edge of the chips is expected to be  
 301 present for an ideal detector because of the finite coverage and the diffusion  
 302 in the drift process.

303 In order to reduce the statistical fluctuations and quantify the tracking  
 304 precision, the pixels were regrouped into larger bins respecting the module  
 305 geometry. After the regrouping procedure, a module plane with  $(4 \times 256) \times 256$   
 306 bins is obtained, as shown in Figure 8 <sup>1</sup>. Bins have a size of  $16 \times 16$  pixels and  
 307 bins with less than 1000 entries are not shown. Due to the presence a so-called  
 308 dike - that was created in the TPX3 post-processing to protect the edges of  
 309 the TPX3 chip - pixels at the edge of the chip were covered and inefficient.  
 310 Therefore, the region of 5 pixels in  $y$  near the edge of each chip was removed.  
 311 For the drift coordinate studies, a region of 10 pixels near the edge of each

---

<sup>1</sup>The mathematical procedure is defined as follows. The original mean residual - before rebinning - is given by  $\text{residual}(i,j)$  where  $i$  runs horizontally and  $j$  vertically. The rebinned result for the  $\text{residual}(4 \times 256, 256)$  is equal to  $\text{residual}(i \% 1024, j \% 256)$ . The mean  $\text{residual}(256, 4 \times 256)$  - discussed later in the paper - is equal to  $\text{residual}(i \% 256, j)$ .

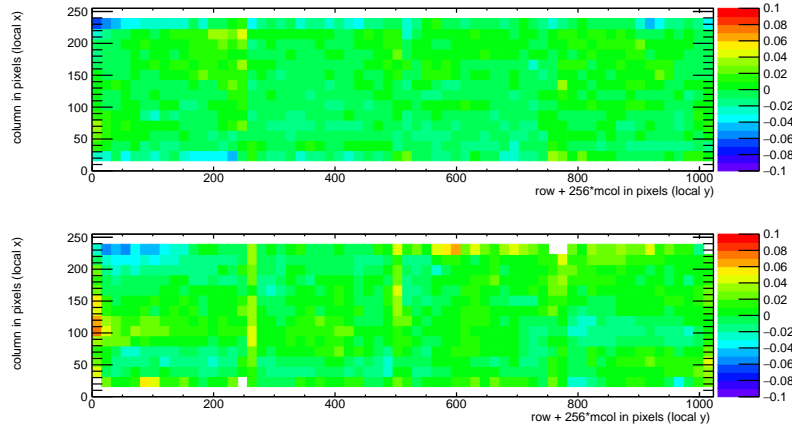


Figure 8: Mean residuals (color coded in mm) in the pixel (top) and drift plane (bottom) for  $B = 0$  T data at the expected hit position.

312 chip in  $x$  and  $y$  was removed. The total number of measurements (bins) in  
 313  $xy$  is 895 and in  $z$  892. One can observe that in the module plane no clear  
 314 systematic deviations are present and conclude that the guard wire voltages  
 315 were on average well tuned. Note that in the quad detector module we had  
 316 no guard wires and deformation corrections had to be applied [2]. The r.m.s.  
 317 of the distribution of the measured mean residual over the surface in the  
 318 pixel plane is  $11 \mu\text{m}$  and in the drift plane  $15 \mu\text{m}$ . Similarly, regrouping the  
 319 module in a plane with  $256 \times (4 \times 256)$  pixel bins, yielded a r.m.s. in the pixel  
 320 plane of  $13 \mu\text{m}$  and  $13 \mu\text{m}$  in the drift coordinate. The expected statistical  
 321 error - obtained by propagating the uncertainties on the residuals - in  $xy$  is  
 322  $4 \mu\text{m}$  and in  $z$   $5 \mu\text{m}$ .

323 In the  $B = 1$  T data set, the electrons will drift mainly along the magnetic  
 324 field lines. Deformations are in that case due to e.g. the non-alignment of the  
 325 electric and magnetic field, giving  $E \times B$  effects. Unfortunately, the statistics

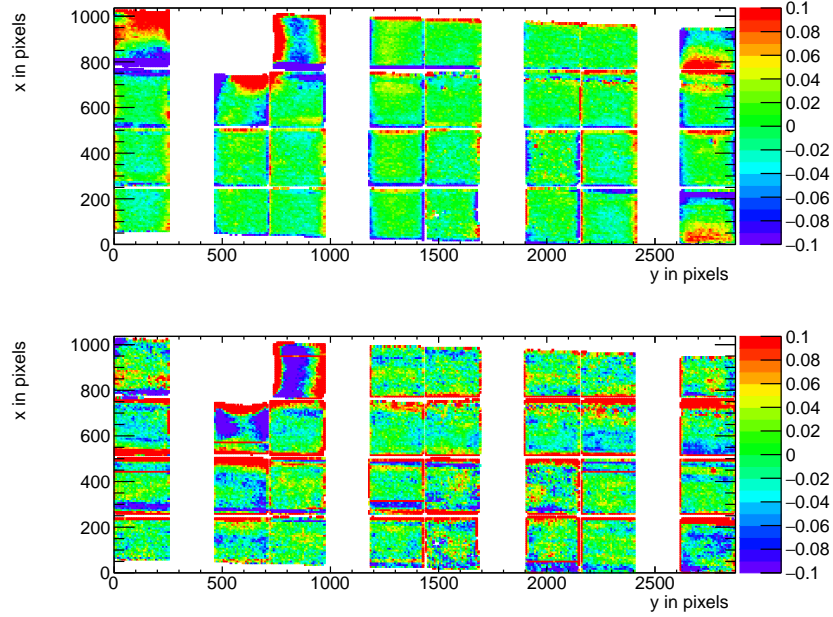


Figure 9: Mean residuals (color coded in mm) in the pixel (top) and drift plane (bottom) for  $B = 1$  T data at the expected hit position.

326 of the telescope tracks that have a matched TPC track was insufficient and  
 327 did not cover the full TPC module plane. Therefore the larger statistics of  
 328 matched and unmatched TPC tracks was used. TPC tracks were required  
 329 to pass angular selection cuts ( $dx/dy$  between -40 and -20 mrad and  $dz/dy$   
 330 between 0 and 14 mrad) and a momentum cut ( $p > 2$  GeV/c and  $q < 0$ ).

331 The mean residuals in the pixel and drift planes are shown in Figure 9 for  
 332 the  $B = 1$  T data set using a large set of runs to cover the whole module. The  
 333 (biased) residuals were calculated with respect to the TPC track prediction.  
 334 Because of limited statistics, bins were grouped into  $16 \times 16$  pixels. Bins with  
 335 less than 100 hits are left out and residuals larger (smaller) than  $+(-)100 \mu\text{m}$   
 336 are shown in red (blue).

337 In Figure 9 the critical areas discussed above - around chip 11, the four  
338 corner chips and chip 16 in the right upper corner edge - can be clearly  
339 observed. For the deformation studies, the hits of these nine chips were  
340 removed. The TPC track fit was redone leaving these hits out of the fit,  
341 thus that they could not bias and affect the results. The TPC plane is well  
342 covered, although one can observe that due to the angle of the beam in the  
343  $xy$  plane the chips in the upper right and lower left corners are not fully  
344 covered.

345 In order to reduce the statistical fluctuations and quantify the tracking  
346 precision, the module was again regrouped in  $(4 \times 256) \times 256$  pixels as de-  
347 scribed above, as shown in Figure 10. Bins have a size of  $16 \times 16$  pixels and  
348 bins with less than 1000 entries are not shown. Similar to the no-field defor-  
349 mation studies, acceptance cuts had to be applied. The region of 16 pixels in  
350  $y$  near the edge of the chips was removed. For the drift coordinate studies,  
351 in addition a region of 10 pixels in  $x$  near the edge of the chip was removed.  
352 The total number of measurements (bins) in  $xy$  is 896 and in  $z$  896. One can  
353 observe that in the module plane no clear systematic deviations are present.  
354 The r.m.s. of the distribution of the measured mean residual over the surface  
355 in the pixel plane is  $13 \mu\text{m}$  and in the drift plane  $19 \mu\text{m}$ . Similarly, regroup-  
356 ing the module in  $256 \times (4 \times 256)$  pixel bins, yielded a r.m.s. in the pixel plane  
357 of  $11 \mu\text{m}$  and  $20 \mu\text{m}$  in the drift coordinate. The expected statistical error  
358 in  $xy$  is  $2 \mu\text{m}$  and in  $z$   $3 \mu\text{m}$ .

359 In summary, the deformation studies for the  $B = 0$  and 1 T data demon-  
360 strate that the systematical uncertainties in  $xy$  are smaller than  $13 \mu\text{m}$  with  
361 and without magnetic field. The systematical uncertainties in  $z$  were smaller

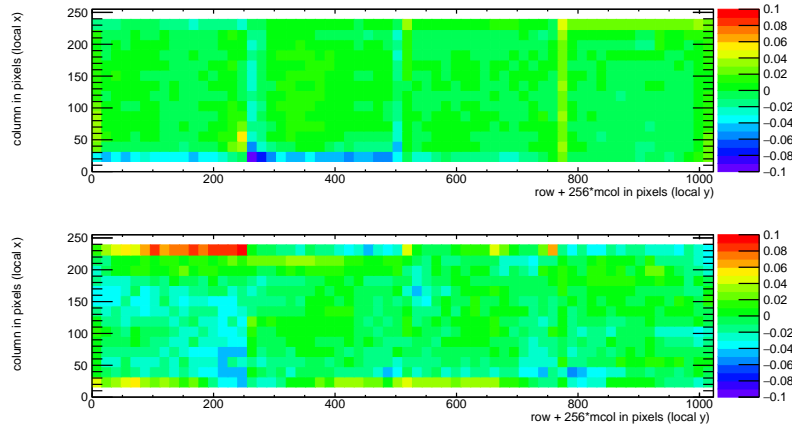


Figure 10: Mean residuals (color coded in mm) in the pixel and drift plane for  $B = 1\text{T}$  data at the expected hit position.

362 than  $15\ \mu\text{m}$  ( $B = 0\ \text{T}$ ) and  $20\ \mu\text{m}$  ( $B = 1\ \text{T}$ ).

#### 363 5.4. Tracking resolution

364 A selected TPC track in the  $B = 0\ \text{T}$  data has on average 1000 hits. The  
 365 tracking precision in the middle of the TPC (at  $y = 1436$  pixels) was derived  
 366 on a track-by-track basis, by propagating the pixel TPC hit uncertainties. It  
 367 was found to be on average  $9\ \mu\text{m}$  in the precision plane and  $13\ \mu\text{m}$  in  $z$ . The  
 368 angular resolution in  $dx/dy$  was on average  $0.19\ \text{mrad}$  and for  $dz/dy$   $0.25$   
 369  $\text{mrad}$ . It is clear that the position resolution in the TPC in the precision  
 370 and drift coordinates is impressive for a track length of (only)  $158\ \text{mm}$ .  
 371 The values are smaller than the uncertainty on the track prediction from  
 372 the silicon telescope of  $26\ \mu\text{m}$  in  $x$  and  $z$  on average that is dominated by  
 373 multiple scattering.

## 374 **6. Single electron efficiency**

375 The distribution of the number of TPC track hits per chip - without  
376 requiring a matched telescope track - are shown in Figure 11 for the data  
377 without magnetic field and for the  $B = 1$  T data. For the  $B = 0$  T data, the  
378 central chips 2,6,7,9,16,17,26 and 27 were selected. For the  $B = 1$  T data,  
379 the same chips plus chips 12,13,20 and 21 were selected.

380 The mean number of hits is measured to be 124 and 89 in the  $B = 0$  T  
381 and 1 T data sets, respectively. The most probable values are respectively  
382 87 and 64. Note that the  $B = 0$  T data have a much larger Landau-like tail  
383 than the 1 T data. Also the fluctuations in the core of the distribution are  
384 larger. The mean time over threshold (ToT) is  $0.68 \mu\text{s}$  for the  $B = 0$  T and  
385  $0.86 \mu\text{s}$  at a  $B = 1$  T data. A typical ToT distribution can be found in Figure  
386 6 of [1] and Figure 5.5 of [4]. The time over threshold is related to the charge  
387 after avalanche multiplication. This means that the mean deposited charge  
388 per pixel is smaller for the 0 T data. The most probable value for the total  
389 deposited charge is similar for both data sets. A possible explanation for  
390 this behavior is that because of the reduced transverse diffusion in the  $B =$   
391 1 T data, the possibility of two primary electrons ending up in a single grid  
392 hole is higher. The mean number of hits is in agreement with the prediction  
393 of 106 electron-ion pairs for a 5 and 6 GeV/c electron at  $B = 0$  T for the  
394 T2K gas by [13], crossing 236 pixels or 12.98 mm and a detector running at  
395 85% single-electron efficiency. The measured single-electron efficiency at this  
396 working point is in agreement with the efficiency vs mean time over threshold  
397 curve that was measured using a Fe source [4].

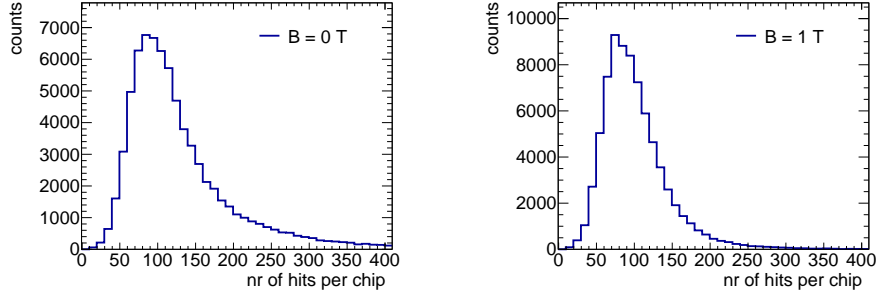


Figure 11: Distribution of the number of TPC track hits per chip for (left)  $B = 0$  T and (right)  $B = 1$  T data.

## 398 7. Conclusion and outlook

399 A TPC module with 32 GridPix chips was constructed and the perfor-  
 400 mance was measured using data taken in a testbeam at DESY in 2021. The  
 401 TPC could be operated reliably and used a 93.6/5.0/1.4 gas mixture (by vol-  
 402 ume) of Ar/ $i$ C<sub>4</sub>H<sub>10</sub>/CO<sub>2</sub> with a small amount of oxygen and water vapour.  
 403 The analysed data were taken at electron beam momenta of 5 and 6 GeV/ $c$   
 404 and at magnetic fields of 0 and 1 T.

405 The result for the transverse diffusion coefficient  $D_T$  is  $(287.2 \pm 0.5)$   
 406  $\mu\text{m}/\sqrt{\text{cm}}$  at  $B = 0$  T and  $D_T$  is  $(120.3 \pm 0.5) \mu\text{m}/\sqrt{\text{cm}}$  at  $B = 1$  T. The  
 407 longitudinal diffusion coefficient  $D_L$  is measured to be  $(251 \pm 14) \mu\text{m}/\sqrt{\text{cm}}$   
 408 at  $B = 0$  T and  $(224 \pm 14) \mu\text{m}/\sqrt{\text{cm}}$  at  $B = 1$  T. Results for the tracking  
 409 systematical uncertainties in  $xy$  were measured to be smaller than  $13 \mu\text{m}$   
 410 with and without magnetic field. The tracking systematical uncertainties in  
 411  $z$  were smaller than  $15 \mu\text{m}$  ( $B = 0$  T) and  $20 \mu\text{m}$  ( $B = 1$  T).

412 The mean number of hits is in agreement with the predictions of [13] and  
 413 a detector running at 85% single-electron efficiency.



414 Not all data were analysed and users are welcome to study them using  
415 the data sets on available on the Grid <sup>2</sup>.

416 The GridPix detector will be further tested and developed in view of a  
417 TPC that will be installed in a heavy ion experiment at the EIC or other  
418 future colliders. A follow-up paper is in preparation on the measured  $dE/dx$   
419 or  $dN/dx$  resolution and other performance topics.

## 420 **Acknowledgements**

421 This research was funded by the Netherlands Organisation for Scientific  
422 Research NWO. The authors want to thank the support of the mechanical  
423 and electronics departments at Nikhef and the detector laboratory in Bonn.  
424 The measurements leading to these results have been performed at the Test  
425 Beam Facility at DESY Hamburg (Germany), a member of the Helmholtz  
426 Association (HGF).

## 427 **References**

- 428 [1] C. Ligtenberg, et al., Performance of a GridPix detector based  
429 on the Timepix3 chip, Nucl. Instrum. Meth. A 908 (2018) 18–23.  
430 arXiv:1808.04565, doi:10.1016/j.nima.2018.08.012.
- 431 [2] C. Ligtenberg, et al., Performance of the GridPix detector quad,  
432 Nucl. Instrum. Meth. A 956 (2020) 163331. arXiv:2001.01540,  
433 doi:10.1016/j.nima.2019.163331.

---

<sup>2</sup>For more information, please contact the corresponding author.

- 434 [3] J. Kaminski, Y. Bilevych, K. Desch, C. Krieger, M. Lupberger, GridPix  
435 detectors - introduction and applications, Nucl. Instrum. Meth. A845  
436 (2017) 233–235. doi:10.1016/j.nima.2016.05.134.
- 437 [4] C. Ligtenberg, A GridPix TPC read out for the ILD experiment at the  
438 future International Linear Collider, Ph.D. thesis, Free University of  
439 Amsterdam (2021). URL  
440 [www.nikhef.nl/pub/services/biblio/theses\\_pdf/thesis\\_C\\_Ligtenberg.pdf](http://www.nikhef.nl/pub/services/biblio/theses_pdf/thesis_C_Ligtenberg.pdf)
- 441 [5] M. Lupberger, Y. Bilevych, H. Blank, D. Danilov, K. Desch, A. Hamann,  
442 J. Kaminski, W. Ockenfels, J. Tomtschak, S. Zigann-Wack, To-  
443 ward the Pixel-TPC: Construction and Operation of a Large Area  
444 GridPix Detector, IEEE Trans. Nucl. Sci. 64 (5) (2017) 1159–1167.  
445 doi:10.1109/TNS.2017.2689244.
- 446 [6] T. Poikela, J. Plosila, T. Westerlund, M. Campbell, M. De Gaspari,  
447 X. Llopart, V. Gromov, R. Kluit, M. van Beuzekom, F. Zappone,  
448 V. Zivkovic, C. Brezina, K. Desch, Y. Fu, A. Kruth, Timepix3: a 65K  
449 channel hybrid pixel read out chip with simultaneous ToA/ToT and  
450 sparse read out, JINST 9 (05) (2014) C05013.  
451 URL <http://stacks.iop.org/1748-0221/9/i=05/a=C05013>
- 452 [7] J. Visser, M. van Beuzekom, H. Boterenbrood, B. van der Heijden, J. I.  
453 Muñoz, S. Kulis, B. Munneke, F. Schreuder, SPIDR: a read-out system  
454 for Medipix3 & Timepix3, Journal of Instrumentation 10 (12) (2015)  
455 C12028. doi:10.1088/1748-0221/10/12/C12028.
- 456 [8] B. van der Heijden, J. Visser, M. van Beuzekom, H. Boterenbrood,

- 457 S. Kulis, B. Munneke, F. Schreuder, SPIDR, a general-purpose read out  
458 system for pixel ASICs, JINST 12 (02) (2017) C02040. doi:10.1088/1748-  
459 0221/12/02/C02040.
- 460 [9] F. Hartjes, A diffraction limited nitrogen laser for detector calibration in  
461 high energy physics, Ph.D. thesis, University of Amsterdam (1990). URL  
462 [www.nikhef.nl/pub/services/biblio/theses\\_pdf/thesis\\_F\\_Hartjes.pdf](http://www.nikhef.nl/pub/services/biblio/theses_pdf/thesis_F_Hartjes.pdf)
- 463 [10] R. Diener et al., The DESY II test beam facility, Nuclear Instru-  
464 ments and Methods in Physics Research. Section A: Accelerators, Spec-  
465 trometers, Detectors and Associated Equipment 922 (2019) 265–286.  
466 arXiv:1807.09328, doi:10.1016/j.nima.2018.11.133.
- 467 [11] P. Baesso, D. Cussans, J. Goldstein, , Journal of Instrumentation 14 (09)  
468 (2019) P09019–P09019. arXiv:2005.00310.  
469 URL <https://doi.org/10.1088/1748-0221/14/09/p09019>
- 470 [12] D. Dannheim, K. Dort, L. Huth, D. Hynds, I. Kremastiotis, J. Kröger,  
471 M. Munker, F. Pitters, P. Schütze, S. Spannagel, T. Vanat, M. Williams,  
472 , Journal of Instrumentation 16 (03) (2021) P03008. doi:10.1088/1748-  
473 0221/16/03/p03008. arXiv:2011.12730.  
474 URL <https://doi.org/10.1088/1748-0221/16/03/p03008>
- 475 [13] R. Veenhof, Garfield - simulation of gaseous detectors, version 9, Refer-  
476 ence W5050 (1984-2010).  
477 URL <https://garfield.web.cern.ch>
- 478 [14] C. Kleinwort, General broken lines as advanced track fitting method,  
479 Nuclear Instruments and Methods in Physics Research Section A: Accel-

480 erators, Spectrometers, Detectors and Associated Equipment 673 (2012)  
481 107–110. doi:10.1016/j.nima.2012.01.024.

482 [15] S. F. Biagi, Monte Carlo simulation of electron drift and diffusion  
483 in counting gases under the influence of electric and magnetic fields,  
484 Nucl. Instrum. Meth. A421 (1-2) (1999) 234–240. doi:10.1016/S0168-  
485 9002(98)01233-9.

486 URL <https://magboltz.web.cern.ch/magboltz>